ADVANCED FUNCTIONAL MATERIALS
www.afm-journal.de

[2.2]Paracyclophane-Substituted Chiral Multiresonant Thermally Activated Delayed Fluorescence Emitters for Efficient Organic Light-Emitting Diodes

Yan Xu, Hassan Hafeez, Jasmin Seibert, Sen Wu, Jhon Sebastian Oviedo Ortiz, Jeanne Crassous, Stefan Bräse, Ifor D. W. Samuel, and Eli Zysman-Colman**

The study reports two pairs of chiral multi-resonant thermally activated delayed fluorescence (MR-TADF) materials PCP-DiKTa and Czp-DiKTa by decorating a known MR-TADF core, DiKTa, with different [2.2]paracyclophane (PCP) based planar chiral groups. PCP-DiKTa shows narrow sky-blue emission with a full width at half maximum (FWHM) of 44 nm, while the emission of Czp-DiKTa is slightly broader with a FWHM of 66 nm and redshifted. Both emitters show high photoluminescence quantum yields of 93 and 99% for PCP-DiKTa and Czp-DiKTa, respectively. Enantiomerically pure samples of both compounds show chiroptical properties in the ground state while only Czp-DiKTa exhibits chiroptical activity in the excited state, with dissymmetry factors ($|g_{PL}|$) of 4×10^{-4}. Organic light-emitting diodes (OLEDs) with PCP-DiKTa and Czp-DiKTa show maximum external quantum efficiencies (EQE_{max}) of 25.7 and 29.2%, with λ_{EL} of 489 and 518 nm, and FWHMs of 53 and 69 nm, respectively. These EQE_{max} values are higher than those of other reported devices employing PCP-based D-A type emitters. This work demonstrates that the PCP moiety is not only a powerful building block to develop planar chiral emitters but one that is compatible with the fabrication of high efficiency devices.

1. Introduction

Organic light-emitting diode (OLED) research has witnessed remarkable growth and dynamism since Tang and Van Slyke first reported an operational OLED at low turn-on voltage back in 1987.[1] OLED displays are now widely found in smartphones, smartwatches, TVs, and automotive screens, offering a panoply of advantages over other display technologies like displaying pure black, having a slim profile, being more energy efficient, and being able to be fabricated on many different substrates including those that are flexible and transparent.[2] Current OLED displays contain anti-glare filters for high-contrast viewing, resulting in 50% efficiency loss after passing through a linear polarizer and a quarter-wave plate. One solution to address this issue is to migrate to circularly polarized OLEDs (CP-OLEDs), implying the use of chiral emitters that emit circularly

Y. Xu, S. Wu, E. Zysman-Colman
Organic Semiconductor Centre
EaStCHEM School of Chemistry
University of St Andrews
St Andrews, Fife KY16 9ST, UK
E-mail: eli.zysman-colman@st-andrews.ac.uk

H. Hafeez, I. D. W. Samuel
Organic Semiconductor Centre
SUPA School of Physics and Astronomy
University of St Andrews
St Andrews, Fife KY16 9SS, UK
E-mail: idws@st-andrews.ac.uk

The ORCID identification number(s) for the author(s) of this article can be found under https://doi.org/10.1002/adfm.202402036

DOI: 10.1002/adfm.202402036

J. Seibert, S. Bräse
Institute of Organic Chemistry (IOC)
Karlsruhe Institute of Technology (KIT)
Kaiserstrasse 12, 76131 Karlsruhe, Germany

J. S. O. Ortiz, J. Crassous
University of Rennes
CNRS
ISCR (Institut des Sciences Chimiques de Rennes)–UMR 6226
Rennes F-35000, France

S. Bräse
Institute of Biological and Chemical Systems (IBCS-FMS)
Karlsruhe Institute of Technology (KIT)
Kaiserstrasse 12, 76131 Karlsruhe, Germany

polarized luminescence (CPL).[3] Generally, the extent of CPL in a chiral emitter is quantified by the luminescence dissymmetry factor, g_{PL}, where $g_{PL} = 2\ (I_L - I_R)/(I_L + I_R) = 4\ (|\mu_e| \cdot |\mu m| \cdot \cos\theta)/(|\mu_e|^2 + |\mu m|^2)$, where I_L and I_R are the left-/right-handed emission intensities, μ_e and μm are the electric and magnetic transition dipole moment vectors, respectively, and θ is the angle between the two. For small organic molecules, the μm is typically much smaller than the μ_e, so the relationship between g_{PL} and the transition dipole moments can be simplified as $g_{PL} = 4 \cdot \mu m \cdot \cos\theta/\mu_e$.[4] This equation implies that the maximum g_{PL} is ±2, and that materials with magnetic dipole-allowed and electric dipole-forbidden transitions would be beneficial to maximize the g_{PL}. In optimized CP-OLEDs, the CPL materials must also be able to harvest efficiently both singlet and triplet excitons, which means that they should emit either by phosphorescence or thermally activated delayed fluorescence (TADF). Thus, there has recently been an intense interest in the development of circularly polarized thermally activated delayed fluorescence (CP-TADF) emitters.[5]

There are two main strategies employed for the design of CP-TADF molecules. One involves designing molecules with an intrinsically chiral TADF skeleton (utilizing point, axial, or planar chirality), while the other entails attaching chiral units to achiral TADF moieties. However, the emission is broad in donor-acceptor CP-TADF compounds as there is large structural relaxation in the excited state. The color purity is insufficient for high-definition display applications hence, narrowband emitters are required. Recently, Hatakeyama and co-workers introduced multiresonant TADF (MR-TADF) compounds that are rigid p- and n-doped polycyclic aromatic hydrocarbon compounds that show narrowband emission.[6] The electron difference densities of the S_1 and T_1 excited states compared to the ground state in these compounds show a pattern of alternating increasing and decreasing electron density that is responsible for the characteristic short-range charge transfer excited state and the suitably small singlet-triplet energy gap, ΔE_{ST}, to enable TADF. Consequently, what is required within this materials space are high-performance CP-MR-TADF emitters. However, examples of CP-MR-TADF emitters remain limited (Figure S1, Supporting Information), especially compared to the thousands of reported TADF emitters reported to date. Devices based on these emitters using a single host often suffer from serious efficiency roll-off owing to the too long exciton lifetimes. One approach to optimize the device performance is to enhance the efficiency of the reverse intersystem crossing (RISC) process by having low-lying excited states of mixed short-range charge-transfer (SRCT) and long-range charge transfer (LRCT) character in the CP-MR-TADF emitters. Our prior work demonstrated that decorating an MR-TADF core with various electron-donating groups can modulate the interplay between the relative energies of the SRCT and LRCT states and their impact on the emission profile.[7] Therefore, the choice of decoration of MR-TADF cores with chiral groups to achieve CPL must also be mindful to retain the desired narrowband emission and to aid in enhancing the RISC kinetics.

[2.2]Paracyclophane (PCP) and its derivatives have emerged as a useful planar chiral skeleton, including in the construction of CP-TADF emitters.[8] Most of the examples of PCP-containing CP-TADF emitters are based on a D-A design. For example, our group integrated a PCP with a nitrogen-heterocycle to produce the bulky carbazolophane (Czp) donor and employed it within the CP-TADF emitter **CzpPhTRZ** (**Figure 1**).[9] The increased steric bulk of the Czp unit compared to carbazole (Cz) induced an increased torsion angle between the donor and the phenylene bridge, resulting in a relatively smaller ΔE_{ST} of 0.16 eV. **(*R*)-CzpPhTrz** emits at λ_{PL} of 470 nm and has a g_{PL} value of 1.2×10^{-3} in toluene, while ***rac*-CzpPhTrz** has a Φ_{PL} of 69% in 10 wt% doped films in DPEPO, which translated into OLEDs that achieved an EQE of 17% at an λ_{EL} at 480 nm; no OLEDs were fabricated using enantiopure samples of the emitter and thus no g_{EL} was measured. Zheng, Ye, Liao et al. subsequently reported a structurally related CP-TADF molecule, **PXZp-Ph-TRZ**, using the same chiral paracyclophane-extended donor strategy as with **CzpPhTrz** but replacing Cz with a stronger phenoxazine (PXZ) donor.[10] The yellow emitter (λ_{PL} = 527 nm) has a much smaller ΔE_{ST} of 0.03 eV than **CzpPhTrz** and a Φ_{PL} of 60% in 10 wt% doped films in CBP. The solution-processed CP-TADF OLEDs showed an EQE_{max} of 7.8%, and using enantiopure emitters the CP-OLEDs displayed a g_{EL} of 4.6×10^{-3}. With a similar skeleton, Chen, Li, Zhang et al. reported a pair of D-chiral π-A type TADF emitter **(*R*/*S*)-PXZ-PT**, with the PCP acting as bridging unit.[11] **(*R*/*S*)-PXZ-PT** emits at λ_{PL} of 565 nm in toluene, has a moderate ΔE_{ST} of 0.19 eV in 2Me-THF, and a high Φ_{PL} of 78% in 10 wt% doped films in CBP; additionally, the g_{PL} was measured to be $\pm 1.9 \times 10^{-3}$ in toluene. The vacuum-deposited CP-OLEDs with **(*R*)-PXZ-PT** exhibited a yellow emission [(λ_{EL} of 557 nm, CIE of (0.44, 0.55)] with an EQE_{max} of 20.1%. In these examples, the emission is broad owing to radiative decay from a LRCT excited state. Recently, Zheng, Liao, Pu et al. attached Czp to two different known MR-TADF cores and reported two CP-MR-TADF emitters.[12] **Czp-tBuCzB**, **Czp-POAB** emit at λ_{PL} of 478 and 498 nm and show narrowband emissions with FWHM of 23 and 36 nm, respectively, in toluene. **Czp-tBuCzB** and **Czp-POAB** have small ΔE_{ST} of 0.09 and 0.13 eV in toluene, and high Φ_{PL} of 98 and 96% in 5 and 8% doped films in 26DCzPPy, respectively. The sky-blue CP-MR-TADF OLEDs showed EQE_{max} of 32.1 and 28.7%, respectively. For the OLED device with **Czp-tBuCzB**, the efficiency roll-off was small of 3.7% at 1000 cd m^{-2}; however, the device with **Czp-POAB** showed a much more severe efficiency roll-off of 28.9% at 1000 cd m^{-2}, which the authors rationalized as due to the planar structure and longer τ_d than that of **Czp-tBuCzB**.

Here, we report two pairs of chiral MR-TADF enantiomers, **PCP-DiKTa** and **Czp-DiKTa** by decorating a known MR-TADF core, **DiKTa**, with different PCP-based planar chiral groups. Owing to the different donor strength of the two chiral groups, the energy of the LRCT state from these donors to the **DiKTa** acceptor will change and this will impact the photophysical and chiroptical properties of the emitters. **PCP-DiKTa** emits at λ_{PL} of 477 nm and has a narrow profile (FWHM of 44 nm), while the emission of **Czp-DiKTa** is red-shifted at λ_{PL} of 501 nm and is broader (FWHM of 66 nm). This implies that Czp is a stronger donor than PCP. Enantiopure **Czp-DiKTa** emitters displayed CPL activity with g_{PL} of $\pm 4 \times 10^{-4}$ while no CPL was detected for **PCP-DiKTa** enantiomers. Both compounds have high Φ_{PL} of 93 and 99% as 2 wt% doped films in 26DCzPPy. The shorter delayed lifetimes, τ_d, of **PCP-DiKTa** and **Czp-DiKTa** than that of the parent **DiKTa** (τ_d = 242 μs) is associated with faster reverse intersystem crossing (RISC) (k_{RISC} of 3.01×10^4 s^{-1} and

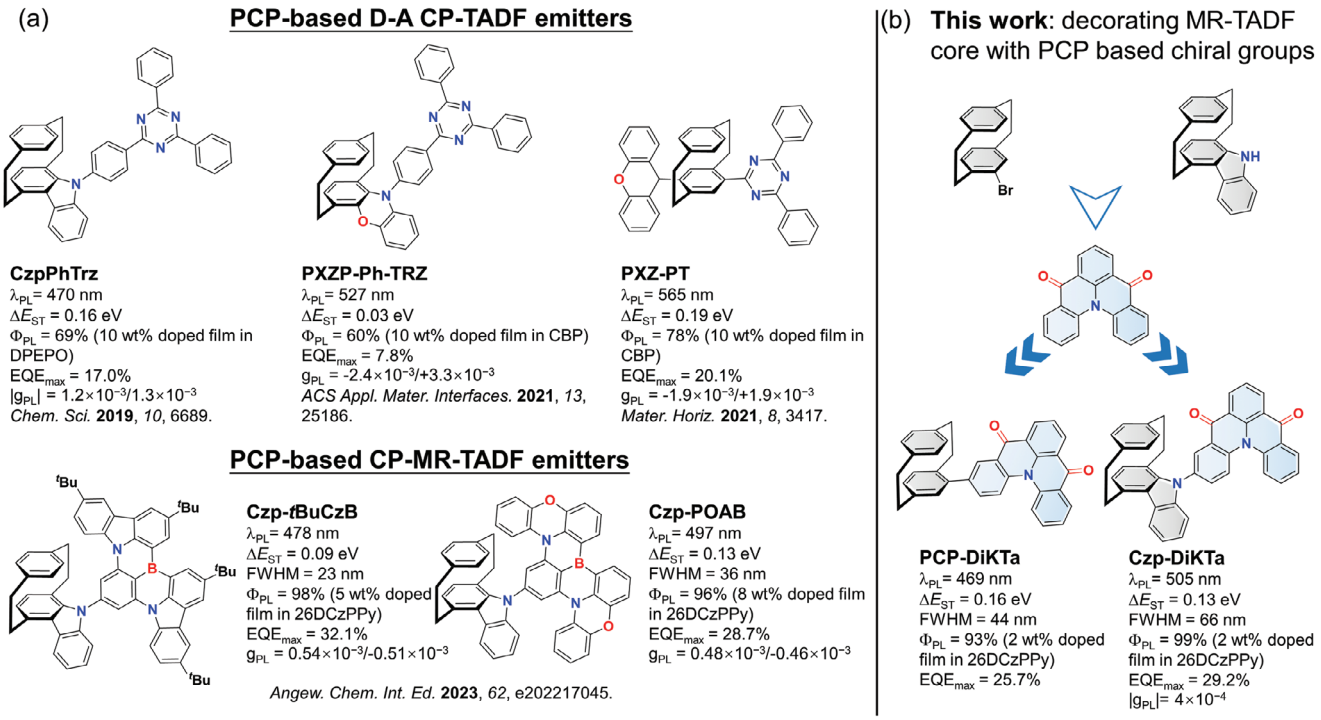

Figure 1. Chemical structures, photophysical, and OLED data of reported PCP-based CP-TADF materials, **PCP-DiKTa** and **Czp-DiKTa** in this work.

4.41 × 10^4 s^{-1}, respectively).[13] The OLEDs with **PCP-DiKTa** and **Czp-DiKTa** showed EQE_{max} of 25.7 and 29.2%. The OLEDs with **Czp-DiKTa** showed a less pronounced efficiency roll-off with EQEs at 100/1000 cd m^{-2} of 25.9/17.1%. This work demonstrates the impact that the electronics of the chiral group has on the photophysics of the emitter and how this ultimately affects the device performance.

2. Results and Discussion

2.1. Molecular Design and Synthesis

The syntheses of **Czp-DiKTa** and **PCP-DiKTa** are outlined in Scheme S1 (Supporting Information). **Czp-DiKTa** was obtained in 66% yield as yellow solid following a palladium-catalyzed Buchwald-Hartwig C-N coupling between **Czp** and **DiKTa-Br**, and **PCP-DiKTa** was synthesized in 48% yield as a yellow solid following a sequence of Miyaura borylation of PCP-Br and Suzuki–Miyaura cross-coupling with **DiKTa-Bpin**. The molecular structures and purity were validated using a combination of ^1H and ^{13}C nuclear magnetic resonance (NMR) spectroscopy, high-resolution mass spectrometry (HRMS), melting point determination, elemental analysis (EA), and high-performance liquid chromatography (HPLC) (Figures S2–S14, Supporting Information). The thermal stability of the two compounds was investigated by thermogravimetric analysis (TGA) and different scanning calorimetry (DSC) (Figure S15, Supporting Information). Both compounds are thermally stable, with a 5% mass loss (T_d) occurring at 390 °C for **PCP-DiKTa** and 362 °C for **Czp-DiKTa**.

2.2. Theoretical Calculations

The ground-state properties of **Czp-DiKTa** and **PCP-DiKTa** were calculated using density functional theory (DFT) at the PBE0/6-31G(d,p) level in the gas phase starting from a geometry generated using Chem3D,[14] while the excited-state calculations were performed using the spin component scaling second-order approximate coupled-cluster (SCS-CC2) method in tandem with the cc-pVDZ basis set, which we have previously shown to be a sufficient level of theory to accurately predict ΔE_{ST} in MR-TADF emitters.[15] In the ground state, the dihedral angle between the stereogenic donor and the **DiKTa** group are 47.6° for **PCP-DiKTa** and 57.5° for **Czp-DiKTa**, which is similar to the dihedral angle of 58° found in the optimized structure of **CzpPhTRZ**.[9] For **PCP-DiKTa**, the HOMO is distributed across the entire molecule while the LUMO is mainly localized on the **DiKTa** fragment (Figure S16, Supporting Information). In contrast, the HOMO of **Czp-DiKTa** is mainly located on Czp donor, with a small degree of electron density on the adjacent arene of the **DiKTa**, while the LUMO is localized on the **DiKTa** fragment. The difference in the HOMO distributions reflects the electron-donating strength of the chiral donor groups. Compared to **DiKTa** (HOMO/LUMO = −6.20/−2.23 eV),[7a] **PCP-DiKTa** (−5.94/−2.24 eV) has a similar LUMO level and a shallower HOMO level while **Czp-DiKTa** (−5.57/−2.36 eV) has a much shallower HOMO level and a deeper LUMO, leading to a much smaller HOMO-LUMO gap. The calculated S_1/T_1 energies are 3.38/3.11 eV for **PCP-DiKTa** and 3.30/3.06 eV for **Czp-DiKTa**, with corresponding ΔE_{ST} values of 0.27 and 0.24 eV, respectively. These values are similar to the calculated S_1/T_1 energies (3.46/3.20 eV) and ΔE_{ST} value

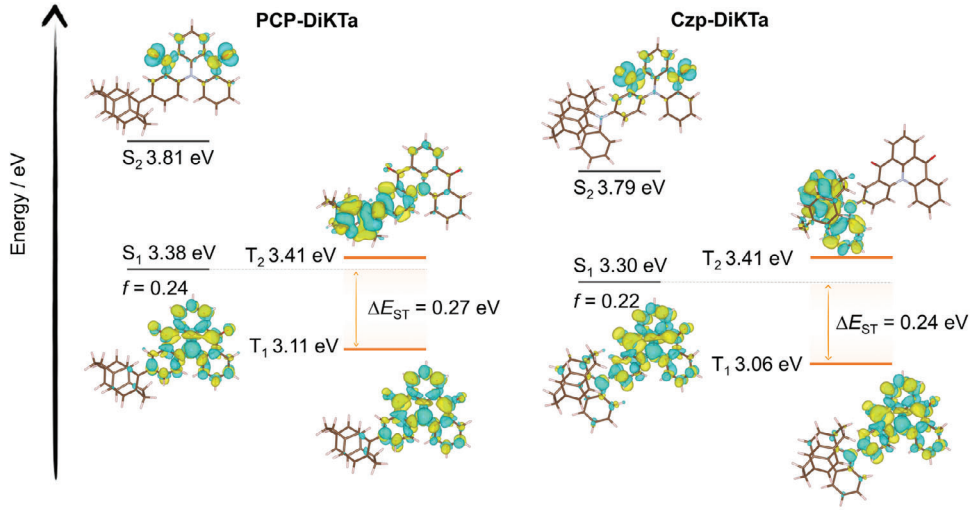

Figure 2. Difference density plots and energies for the S_1, S_2, T_1, and T_2 of **PCP-DiKTa** and **Czp-DiKTa** calculated at SCS-CC2/cc-pVDZ in the gas phase (ISO value = 0.02). The blue color represents an area of decreasing electron density, and the yellow color represents an increased electron density between the ground and excited states.

(0.26 eV) of **DiKTa**.[13] The oscillator strengths for the S_0-S_1 transitions for **PCP-DiKTa** (0.24) and **Czp-DiKTa** (0.22) are larger than that of **DiKTa** (0.20), implying that these two emitters will be brighter. The difference density plots for the S_1, S_1, T_1, and T_2 excited states are shown in **Figure 2**. The first singlet and triplet excited states show a pattern of alternating increasing and decreasing electron density that is typical of excited states of short-range charge transfer (SRCT) character; there is a small contribution to the S_1 difference density plot originating from the chiral donors. The S_2 state for both molecules has n–π^* character, while the electron density of the T_2 is located mainly on the donor moieties. The different orbitals involved in the S_2/T_2 states compared to the S_1/T_1 states contribute to the spin-orbit coupling (SOC). The SOC matrix elements (SOCME) at the optimized T_1 geometry between S_1 and T_2 are 4.15 and 0.45 cm^{-1} for **PCP-DiKTa** and **Czp-DiKTa**, respectively, which are significantly larger than that between S_1 and T_1 (0.27 and 0.26 cm^{-1}, respectively, Figure S16, Supporting Information).

2.3. Optoelectronic Properties

The electrochemical properties of the two emitters were investigated by cyclic voltammetry (CV) and differential pulse voltammetry (DPV) in deaerated DCM with 0.1 M tetra-*n*-butylammonium hexafluorophosphate as the supporting electrolyte (Figure S17, Table S1, Supporting Information). Both compounds show irreversible oxidation waves, which are assigned to the oxidation of either the whole skeleton for **PCP-DiKTa** or the **Czp** for **Czp-DiKTa** according to an analysis of the HOMO distribution from DFT calculation. Both compounds show reversible reduction waves, which correspond to the reduction of the **DiKTa** core according to DFT calculations.[7b] The E_{ox}/E_{red} values were determined from the peaks of the DPVs. Compared to **DiKTa** (E_{ox}/E_{red} = 1.78/−1.34 V), both **PCP-DiKTa** (1.58/−1.29 V) and **Czp-DiKTa** (1.14/−1.27 V) have similar, albeit slightly anodically shifted reduction potentials while their oxidation potentials are cathodically shifted. The corresponding HOMO-LUMO gaps are 2.87 and 2.41 eV, respectively, and the trends in the electrochemical data largely mirror those in the DFT study.

The UV–vis absorption and steady-state photoluminescence (PL) spectra recorded at room temperature in dilute toluene are shown in **Figure 3a**. There is a similar band at 445 nm in the absorption spectra, to the SRCT transitions centered on the **DiKTa** core. Compared to **DiKTa** (λ_{abs} = 433 nm),[13] the SRCT band of **PCP-DiKTa** and **Czp-DiKTa** is slightly red-shifted and broader, indicating that this transition has an admixture of LRCT and SRCT character. The lower molar extinction coefficient (ϵ) of 7.56 × 10^3 M^{-1} cm^{-1} for this band in **Czp-DiKTa** is due to the more twisted geometry between the **Czp** donor and **DiKTa** compared to **PCP-DiKTa** (ϵ of 28.43 × 10^3 M^{-1} cm^{-1}), which itself is similar in magnitude to the SRCT band in **DiKTa** (ϵ of 22.06 × 10^3 M^{-1} cm^{-1}).[16] This is analogous behavior to that observed in **Cz-DiKTa** and **DMAC-DiKTa**, both of which display a similarly twisted structure to **Czp-DiKTa** (ϵ of 16.92 × 10^3 and 12.50 × 10^3 M^{-1} cm^{-1}, respectively),[7a] while the CT band in **CzpPhTrz** has a lower ϵ of 4.65 × 10^3 M^{-1} cm^{-1} as the **Czp** group is more poorly electronically coupled to the **TRZ** acceptor.

Both compounds have unstructured PL spectra in toluene with λ_{PL} of 469 nm for **PCP-DiKTa** and 505 nm for **Czp-DiKTa**. Compared to the PL spectra of **DiKTa**, **Cz-DiKTa**, **DMAC-DiKTa**, and **CzpPhTrz** (FWHMs of 27, 54, 94, and 80 nm, respectively),[7a] that of **PCP-DiKTa** (FWHM of 37 nm) is slightly broader than that of **DiKTa**, while that of **Czp-DiKTa** (FWHM of 66 nm) is slightly broader than that **Cz-DiKTa**, and narrower than that **DMAC-DiKTa** and **CzpPhTrz**. The PL spectra of **PCP-DiKTa** show a small degree of positive solvatochromism (Figure S18, Supporting Information), which is consistent with an excited state of SRCT character that is emblematic of MR-TADF emitters. By contrast, there is a much stronger positive solvatochromism in the PL spectra of **Czp-DiKTa**, reflecting an excited state with significant LRCT character. Indeed, in tetrahydrofuran and ethyl

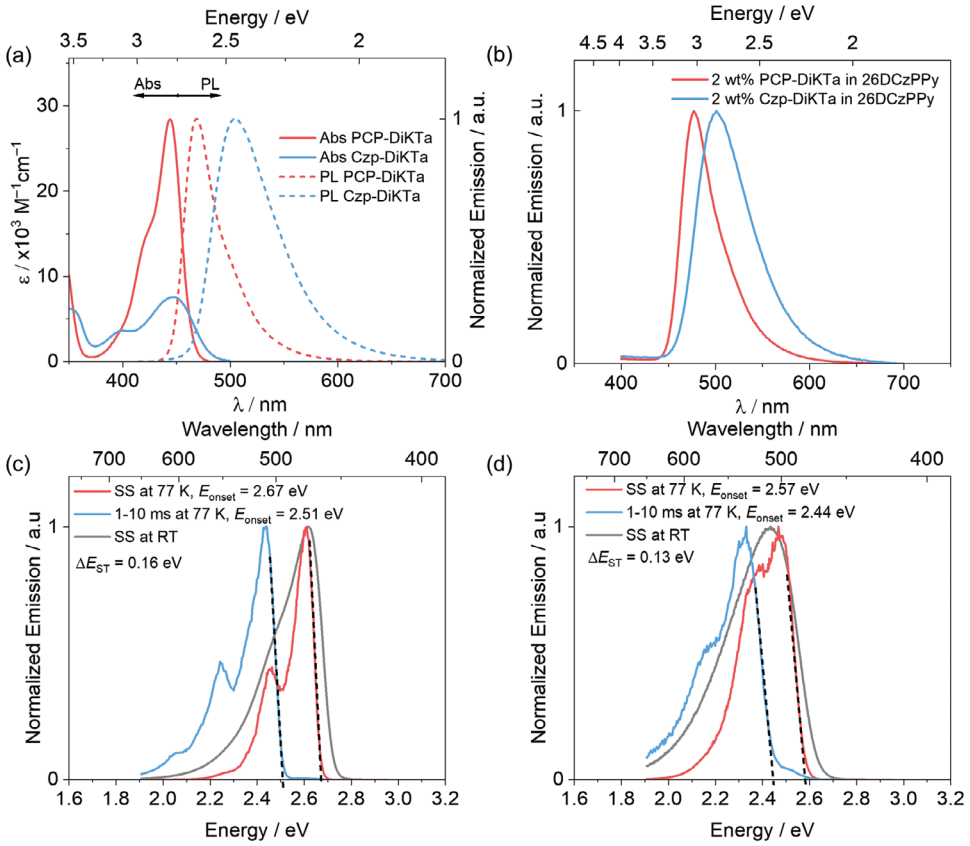

Figure 3. a) UV–vis absorption and steady-state PL spectra recorded in aerated toluene at 298 K (λ_{exc} = 340 nm). b) Steady-state PL spectra (λ_{exc} = 343 nm) in 2 wt% doped films. c) Steady-state PL spectra of **PCP-DiKTa** at 77 K and room temperature (λ_{exc} = 353 nm), and phosphorescence spectra at 77 K (1–10 ms, λ_{exc} = 353 nm) in toluene. d) Steady-state PL spectra of **Czp-DiKTa** at 77 K and room temperature (λ_{exc} = 365 nm), and phosphorescence spectra at 77 K (1–10 ms, λ_{exc} = 365 nm) in toluene; concentration: 1×10^{-5} M.

acetate, **Czp-DiKTa** shows dual emission emanating from the LRCT and SRCT states. The S_1 and T_1 energies of both compounds were determined from the onsets of the steady-state PL and phosphorescence spectra at 77 K in toluene (Figure 3c,d). These are 2.67/2.51 eV for **PCP-DiKTa** and 2.57/2.44 eV for **Czp-DiKTa**, resulting in ΔE_{ST} of 0.16 and 0.13 eV for **PCP-DiKTa** and **Czp-DiKTa**, respectively. These values are smaller than those of **DiKTa** (0.22 eV), **Cz-DiKTa** (0.20 eV) and **DMAC-DiKTa** (0.21 eV). The Φ_{PL} of **PCP-DiKTa** and **Czp-DiKTa** in degassed toluene solutions are 36 and 37%, respectively, which are higher than that of **DiKTa** in toluene (26%); these decrease to 32 and 30% upon exposure to oxygen. The time-resolved emission decays do not show any delayed fluorescence, with lifetimes, τ_{PL}, of 6.2 and 13.9 ns (Figure S19, Supporting Information). In contrast, **DiKTa** shows multiexponential kinetics containing both prompt and delayed PL lifetimes in toluene, with τ_p and τ_d of 5.1 ns and 23 µs, respectively.[16]

We then explored the photophysical properties of the two emitters in an OLED-relevant host, 2,6-bis(3-(carbazol-9-yl)phenyl)pyridine (26DCzPPy), which is one that is bipolar and thus can mediate both the transport of holes and electrons within the emissive layer of the device;[17] additionally, it has suitably high triplet energy of 2.71 eV to confine the excitons onto the emitter.[18] We studied the photophysical properties of these films as a function of emitter doping concentrations from 2 to 20 wt% (Figure S20, Supporting Information). Both compounds displayed only modest red-shifting of their PL in this doping range, which implies little aggregation. Both emitters showed the highest Φ_{PL} at 2 wt% doped films at 93% for **PCP-DiKTa** and 99% for **Czp-DiKTa** under N_2, values which then reduced to 66 and 73% in air, respectively (Tables S2 and S3, Supporting Information). Therefore, we used 2 wt% emitter doped 26DCzPPy films for the subsequent photophysical measurements. The steady-state emissions of **PCP-DiKTa** and **Czp-DiKTa** peak at λ_{PL} at 477 and 501 nm, with FWHMs of 44 and 66 nm, respectively (Figure 3b, **Table 1**). Multiexponential decay kinetics under vacuum were observed, with prompt fluorescence lifetimes, τ_p, for **PCP-DiKTa** and **Czp-DiKTa** of 6.4 and 11.7 ns, respectively, and delayed fluorescence lifetimes, τ_d, of 179 and 140 µs, respectively (**Figure 4**). The k_{RISC} of **PCP-DiKTa** and **Czp-DiKTa** are 3.01×10^4 and 4.41×10^4 s^{-1}, respectively, which are faster than that of **DiKTa** (2.52×10^4 s^{-1}).[13] Full kinetics parameters are summarized in Table S4 (Supporting Information). Temperature-dependent time-resolved PL decay behavior revealed the expected increase in the contribution from the delayed emission with increasing temperature that defines TADF (Figure 4). The ΔE_{ST} values estimated from the difference in energy between the onsets of

Table 1. Photophysical properties of **PCP-DiKTa** and **Czp-DiKTa**.

	λ_{abs} [a] /nm	λ_{PL} [a] /nm	λ_{PL} [b] /nm	FWHM [b] /nm	Φ_{PL} [a] /%	Φ_{PL} [b] /%	τ_p [b),c] /ns	τ_d [b),c] /µs	S_1/T_1 [d] /eV	ΔE_{ST} [d] /eV
PCP-DiKTa	444	469	477	44	36(32)	93(66)	6.4	179	2.67/2.51	0.16
Czp-DiKTa	446	505	501	66	37(30)	99(73)	11.7	140	2.57/2.44	0.13

[a] In toluene at 298 K; [b] spin-coated 2 wt% thin films in 26DCzPPy (λ_{exc} = 343 nm); [c] Average lifetime ($\tau_{avg} = \Sigma A_i\tau_i^2/\Sigma A_i\tau_i^2$, where A_i is preexponential for lifetime τ_d). Prompt and delayed emission were measured by TCSPC (λ_{exc} = 379 nm) and MCS (λ_{exc} = 343 nm), respectively; [d] Determined from the onset of the SS PL and phosphorescence spectra in toluene at 77 K.

the steady-state PL and phosphorescence spectra at 77 K are 0.19 eV for **PCP-DiKTa** and 0.17 eV for **Czp-DiKTa**, which are slightly larger than those in toluene (Figure S21, Supporting Information).

2.4. Chiroptical Properties

The experimental electronic circular dichroism (ECD) spectra of the enantiomeric compounds were measured in toluene solutions (10^{-4} M); the ***(1st)/(2nd)***-enantiomers refer to the ***1st*** and ***2nd*** enantiomers according to retention time that are detected by chiral HPLC (Figures S5 and S13, Supporting Information). They displayed the typical mirror-image relationship (**Figure 5**a,b). In the case of ***(2nd)*-PCP-DiKTa**, Cotton effects were observed at 309 ($\Delta\epsilon = -46$ M^{-1} cm^{-1}), 343 (+1.3), and 371 nm (+3.2). For ***(2nd)*-Czp-DiKTa** enantiomer, Cotton effects were observed at 287 ($\Delta\epsilon = -13.7$ M^{-1} cm^{-1}), 306 (+10), 318 (−4.9), 354 (−1.9), 367 (−1.7), 377 (+2), 393 (+6.8), and 452 nm (+2.5).

The circularly polarized luminescence (CPL) was then examined. The CPL spectra were recorded in dilute solutions of toluene at r.t and are shown in Figure 5c for ***(1st)/(2nd)*-Czp-DiKTa** enantiomers. These were found to display mirror-image CPL signals at 507 nm with photoluminescence dissymmetry factors g_{PL} of $\approx\pm4 \times 10^{-4}$ and with signs similar to the low-energy ECD-active bands, i.e., positive for ***(2nd)*-Czp-DiKTa** (see g_{PL} plots in Figure 5d). However, no clear CPL signals could be measured for ***(1st)/(2nd)*-PCP-DiKTa**. Since the emission process mirrors the low-energy absorption one, the absence of CPL signal may be explained by the fact that for **PCP-DiKTa** the band at 445 nm, corresponding to the HOMO-LUMO transition, does not display ECD activity (Figure 5a). The magnitude of the g_{PL} of **Czp-DiKTa** is similar to those reported for other CP-MR-TADF emitters; for example, ***(R)*/*(S)*-Czp-tBuCzB** and ***(R)*/*(S)*-Czp-POAB** have g_{PL} of

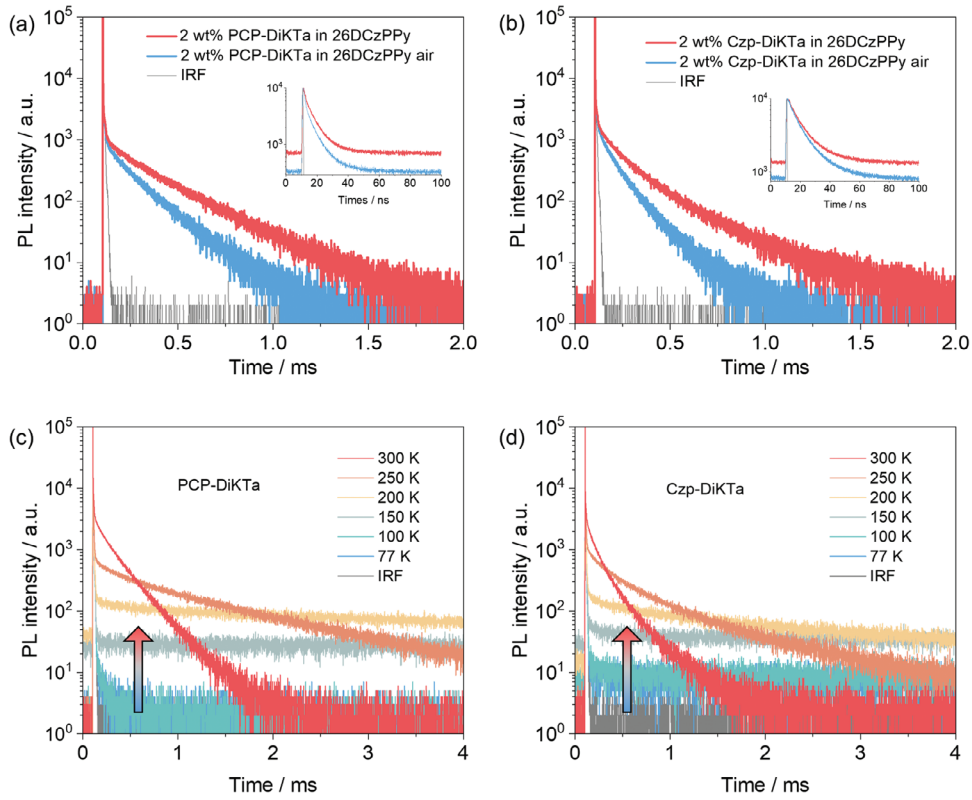

Figure 4. Time-resolved PL decays (λ_{exc} = 343 nm) of a) **PCP-DiKTa** and b) **Czp-DiKTa** in 2 wt% doped film in 26DCzPPy (inset figures are the time-resolved PL decays of the prompt component, λ_{exc} = 375 nm). Temperature-dependent time-resolved PL decay of c) **PCP-DiKTa** and d) **Czp-DiKTa** in 2 wt% doped film in 26DCzPPy, λ_{exc} = 343 nm.

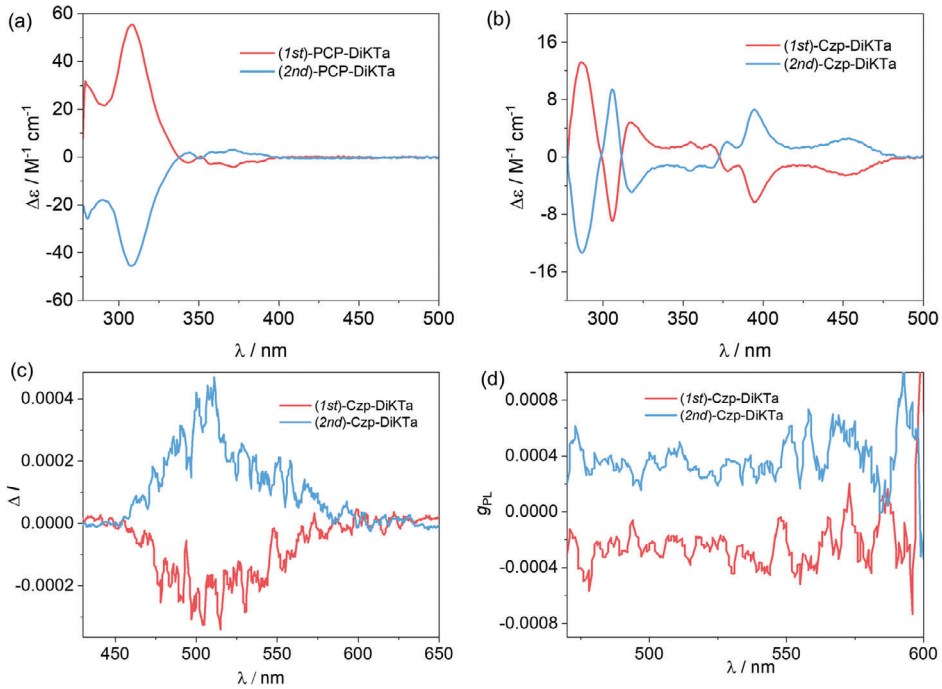

Figure 5. Experimental ECD spectra of a) ***(1st)/(2nd)*-PCP-DiKTa** and b) ***(1st)/(2nd)*-Czp-DiKTa** in toluene. c) Experimental CPL spectra and d) g_{PL} values of ***(1st)/(2nd)*-Czp-DiKTa** in toluene (λ_{exc} = 444 nm). ***(1st)/(2nd)***-enantiomers refer to the 1st and 2nd enantiomers eluted by chiral HPLC.

$5.4/-5.1 \times 10^{-4}$ and $4.8/-4.6 \times 10^{-4}$ in toluene, respectively. The g_{PL} values are, however, slightly lower than other PCP-based D-A TADF emitters, which usually have dissymmetry values on the order of 10^{-3}.[12]

2.5. Organic Light-Emitting Diodes (OLEDs)

We next fabricated vacuum-deposited OLEDs. The OLED device stack and the chemical structures of the organic layers are shown in **Figure** 6a,b, respectively. The OLEDs consist of indium tin oxide (ITO)/1,4,5,8,9,11-hexaazatriphenylenehexacarbonitrile (HATCN, 5 nm)/1,1-bis[(di-4-tolylamino)phenyl]cyclohexane (TAPC, 45 nm)/1,3-bis(*N*-carbazolyl)benzene (mCP, 5 nm)/26DCzPPy as host (20 nm) with **PCP-DiKTa**, and **Czp-DiKTa** as emitter dopants/1,3,5-tris(3-pyridyl-3-phenyl)benzene (TmPyPB, 45 nm)/lithium fluoride (LiF, 1 nm)/aluminum (Al, 100 nm). Here, HATCN was used as the hole injection layer, TAPC as the hole transport layer, mCP as an exciton blocking layer, TmPyPB as electron transport layer, and LiF to reduce the work function of the top Al electrode. The devices were made with 2, 5, 10, and 15 wt% doping of **PCP-DiKTa** or **Czp-DiKTa**, with the lower concentrations of emitter giving higher efficiency, helped by higher Φ_{PL} (Table S3, Supporting Information). The current density–voltage–luminance (JVL) characteristics of the OLEDs with 2 and 5 wt% doping of **PCP-DiKTa** and **Czp-DiKTa** are shown in Figure 6c and **Table 2**. All devices had turn-on voltages of between 3.8 and 4.1 V. For the OLED with **PCP-DiKTa**, the 2 wt% device showed the highest EQE_{max} of 25.7% in accordance with the high Φ_{PL} for this concentration. The EQE decreased to 19.1% at 100 cd m^{-2} and to 8.7% at 1000 cd m^{-2} (Figure 6d). The OLED emitted at λ_{EL} at 489 nm (Figure 6e) with a FWHM of 53 nm, which is close to the PL (λ_{PL} of 477 nm; FWHM of 44 nm) of the emitter molecule. The CIE coordinates are (0.162, 0.450), Figure 6f. With an increase in the doping concentration of the emitter to 5 wt%, the EQE_{max} of the device dropped to 20.5%, which is consistent with the drop in Φ_{PL} from 93% (for the 2 wt% doped film) to 83% (for the 5 wt% doped film). The devices with higher concentrations of the emitter are shown in Figure S22 (Supporting Information).

The OLEDs with **Czp-DiKTa** (5 wt%) showed a very high EQE_{max} of 29.2%, which decreased to 25.9% at 100 cd/m^2 and a high EQE of 17.1% at 1000 cd/m^2 as shown in Figure 6d and Table 2. Thus, compared to the device with **PCP-DiKTa**, the EQE_{max} was both higher and the efficiency roll-off less severe in the device with **Czp-DiKTa**. The device emitted at λ_{EL} at 518 nm (FWHM of 69 nm), Figure 6e, which was slightly redshifted compared to the PL (λ_{PL} = 501 nm; FWHM = 66 nm). The corresponding CIE coordinates are (0.256, 0.610). With 2 wt% of the emitter concentration, a slightly lower EQE_{max} of 27.8% was recorded despite the higher Φ_{PL} (99 and 97% for the 2 and 5 wt% doped films, respectively). The EQE_{100}/EQE_{1000} were 23.1/15.0%, reflecting a more severe efficiency roll-off in this device. Overall, the efficiency roll-off for **Czp-DiKTa** devices at all concentrations (Figure S22, Supporting Information) was less pronounced. Photographs of the OLEDs with **PCP-DiKTa** and **Czp-DiKTa** are shown in Figure 6e, respectively.

3. Conclusion

In summary, we have successfully developed two chiral MR-TADF emitters, **PCP-DiKTa** and **Czp-DiKTa**, by decorating **DiKTa** with two different chiral groups Czp and PCP, and explored how the donor strength modulated the energy of mixed

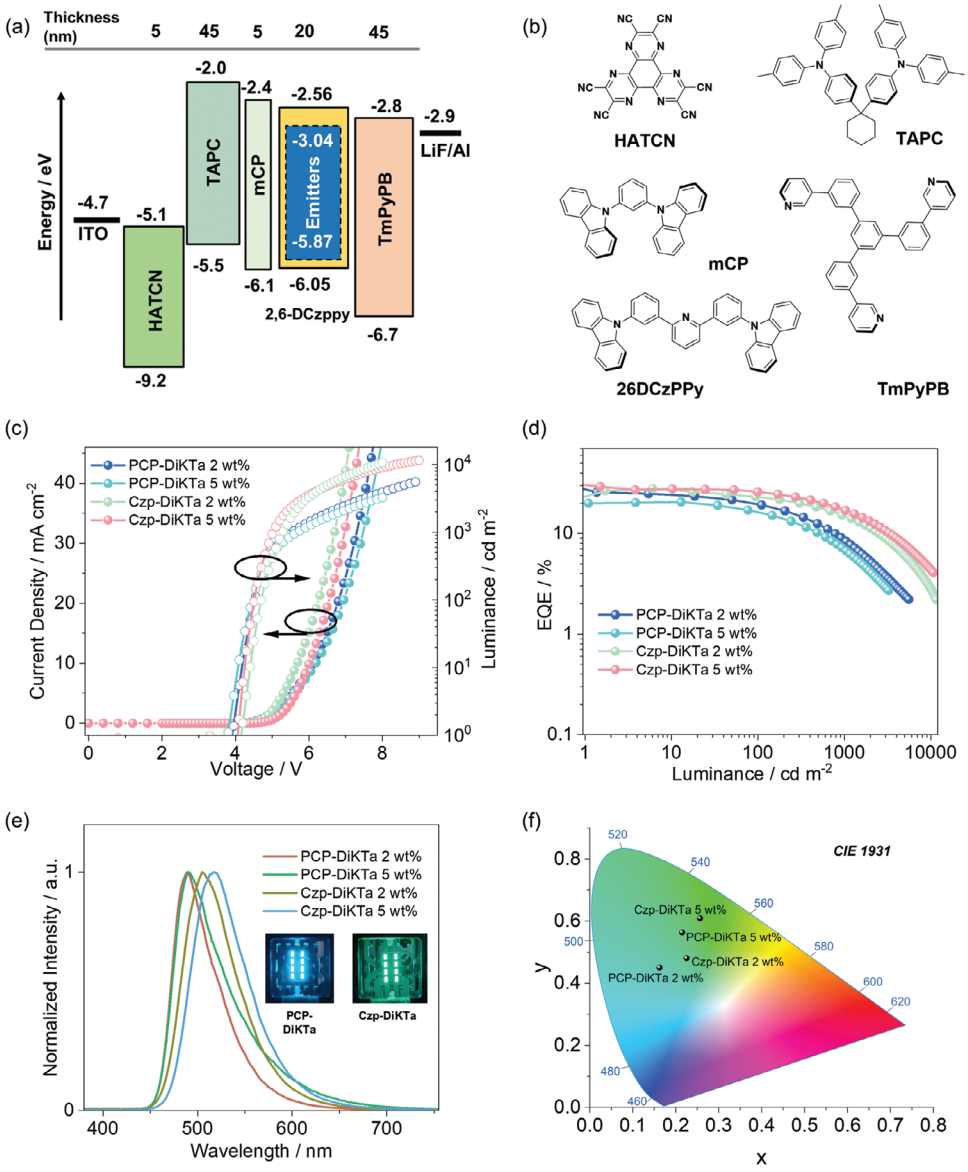

Figure 6. a) Schematic of the OLED stack; b) Chemical structures of the materials used in the device; c) Current density-voltage-luminescence (JVL) characteristics; d) External quantum efficiency (EQE) versus luminescence; e) Electroluminescence spectra, inset figures are photographs of the OLEDs fabricated with **PCP-DiKTa** 2 wt% and **Czp-DiKTa** 2 wt%; f) CIE coordinates of the devices.

Table 2. OLED performance.

	x[a] /wt%	λ_{EL}[b] /nm	FWHM[c] nm	V_{on}[d] /V	L_{max}[e] /cd m^{-2}	$EQE_{max/100/1000}$[f] /%	CIE[g] /x, y
PCP-DiKTa	2	489	53	3.9	5558	25.7/19.1/8.7	0.162, 0.450
	5	490	61	3.8	3248	20.5/16.3/6.9	0.225, 0.480
Czp-DiKTa	2	505	63	4.1	11 536	27.8/23.1/15.0	0.214, 0.563
	5	518	69	4.2	10 689	29.2/25.9/17.1	0.256, 0.610

[a] Emitter doping concentration in the EML; [b] The electroluminescence peak; [c] Full width at half-maximum; [d] Turn-on voltage; [e] Maximum luminance; [f] Maximum external quantum efficiency/EQE at 100 cd m^{-2}/EQE at 1000 cd m^{-2}; [g] Commission Internationale de l'Éclairage (CIE) coordinates.

SRCT and LRCT state, thereby influencing the photophysical properties and corresponding device performance. The resulting compounds **PCP-DiKTa** and **Czp-DiKTa** showed high Φ_{PL} of 93% and 99%, moderate ΔE_{ST} of 0.19 and 0.17 eV, and shorter delayed lifetimes of 179 and 140 µs in 2 wt% doped films in 26DCzPPy than that of the parent DiKTa. Meanwhile, **(*1st*)/(*2nd*)-PCP-DiKTa** and **(*1st*)/(*2nd*)-Czp-DiKTa** displayed mirror-image ECD spectra in toluene solutions and CPL activity was found for **(*1st*)/(*2nd*)-Czp-DiKTa** only, with g_{PL} values of $\pm 4 \times 10^{-4}$ in toluene solutions. OLEDs with **PCP-DiKTa** and **Czp-DiKTa** showed narrow EL spectra with FWHMs of 53 and 69 nm, and high EQE_{max} of 25.7% and 29.2%. Notably, device with **Czp-DiKTa** showed a less pronounced efficiency roll-off, with EQEs at 100/1000 cd m^{-2} of 25.9/17.1%. This study serves as an illustrative example of how a CP-TADF emitter can be tailored to achieve narrow emission and superior device performance, mitigating efficiency roll-off concerns.

Supporting Information

Supporting Information is available from the Wiley Online Library or from the author.

Acknowledgements

Y.X. and H.H. contributed equally to this work. The authors are grateful to the EPSRC for financial support (grant EP/W0151371/1 and EP/W007517/1). Y.X. thanks the China Scholarship Council (202106310038) for support. J.S. thanks the Jürgen Manchot Foundation, the Karlsruhe School of Optics and Photonics, and Dr. Erik Strandberg and Bianca Posselt, for their help in ECD measurements. The authors thank the European Commission Research Executive Agency (Grant Agreement number: 101073045– TADFsolutions – HORIZON-MSCA-2021-DN) and the EPSRC (EP/X026175/1) for financial support. The authors acknowledge the Ministère de l'Enseignement Supérieur et de la Recherche and the Centre National de la Recherche Scientifique (CNRS). Dr. Ludovic Favereau is thanked for his technical support.

Conflict of Interest

The authors declare no conflict of interest.

Data Availability Statement

The research data supporting this publication can be accessed at https://doi.org/10.17630/44d40b58-448d-4e10-baf0-73e2c35dc341.

Keywords

[2.2]Paracyclophane, circularly polarized luminescence, multiresonant thermally activated delayed fluorescence, organic light-emitting diodes

Received: February 1, 2024
Revised: February 29, 2024
Published online:

[1] G. Hong, X. Gan, C. Leonhardt, Z. Zhang, J. Seibert, J. M. Busch, S. Brase, *Adv. Mater.* **2021**, *33*, 2005630.
[2] Y. Huang, E. L. Hsiang, M. Y. Deng, S. T. Wu, *Light Sci. Appl.* **2020**, *9*, 105.
[3] W. R. Kitzmann, J. Freudenthal, A. M. Reponen, Z. A. VanOrman, S. Feldmann, *Adv. Mater.* **2023**, *35*, 2302279.
[4] Y. Zhang, S. Yu, B. Han, Y. Zhou, X. Zhang, X. Gao, Z. Tang, *Matter* **2022**, *5*, 837.
[5] a) Y. Xu, Q. Wang, X. Song, Y. Wang, C. Li, *Chem. - Eur. J.* **2023**, *29*, 202203414; b) M. Li, C.-F. Chen, *Org. Chem. Front.* **2022**, *9*, 6441.
[6] T. Hatakeyama, K. Shiren, K. Nakajima, S. Nomura, S. Nakatsuka, K. Kinoshita, J. Ni, Y. Ono, T. Ikuta, *Adv. Mater.* **2016**, *28*, 2777.
[7] a) S. Wu, W. Li, K. Yoshida, D. Hall, S. Madayanad Suresh, T. Sayner, J. Gong, D. Beljonne, Y. Olivier, I. D. W. Samuel, E. Zysman-Colman, *ACS Appl. Mater. Interfaces* **2022**, *14*, 22341; b) S. Wu, A. Kumar Gupta, K. Yoshida, J. Gong, D. Hall, D. B. Cordes, A. M. Z. Slawin, I. D. W. Samuel, E. Zysman-Colman, *Angew. Chem., Int. Ed.* **2022**, *61*, 202213697.
[8] J. M. Teng, D. W. Zhang, C. F. Chen, *ChemPhotoChem* **2021**, *6*, 202100228.
[9] N. Sharma, E. Spuling, C. M. Mattern, W. Li, O. Fuhr, Y. Tsuchiya, C. Adachi, S. Bräse, I. D. W. Samuel, E. Zysman-Colman, *Chem. Sci.* **2019**, *10*, 6689.
[10] C. Liao, Y. Zhang, S. H. Ye, W. H. Zheng, *ACS Appl. Mater. Interfaces* **2021**, *13*, 25186.
[11] D. W. Zhang, J. M. Teng, Y. F. Wang, X. N. Han, M. Li, C. F. Chen, *Mater. Horiz.* **2021**, *8*, 3417.
[12] X. J. Liao, D. Pu, L. Yuan, J. Tong, S. Xing, Z. L. Tu, J. L. Zuo, W. H. Zheng, Y. X. Zheng, *Angew. Chem., Int. Ed.* **2023**, *62*, 202217045.
[13] S. Wu, L. Zhang, J. Wang, A. Kumar Gupta, I. D. W. Samuel, E. Zysman-Colman, *Angew. Chem., Int. Ed.* **2023**, *62*, 202305182.
[14] S. M. Kerwin, *J. Am. Chem. Soc.* **2010**, *132*, 2466.
[15] a) D. Hall, J. C. Sancho-García, A. Pershin, G. Ricci, D. Beljonne, E. Zysman-Colman, Y. Olivier, *J. Chem. Theory Comput.* **2022**, *18*, 4903; b) A. Pershin, D. Hall, V. Lemaur, J. C. Sancho-Garcia, L. Muccioli, E. Zysman-Colman, D. Beljonne, Y. Olivier, *Nat. Commun.* **2019**, *10*, 597.
[16] D. Hall, S. M. Suresh, P. L. dos Santos, E. Duda, S. Bagnich, A. Pershin, P. Rajamalli, D. B. Cordes, A. M. Z. Slawin, D. Beljonne, A. Köhler, I. D. W. Samuel, Y. Olivier, E. Zysman-Colman, *Adv. Opt. Mater.* **2020**, *8*, 1901627.
[17] S.-J. Su, C. Cai, J. Kido, *Chem. Mater.* **2010**, *23*, 274.
[18] T. Zhang, C. Shi, C. Zhao, Z. Wu, N. Sun, J. Chen, Z. Xie, D. Ma, *J. Mater. Chem. C* **2017**, *5*, 12833.